

Fig. 1. Example scenario from the *round* dataset. The color of the agents represents how they are scored in the prediction task. The blue vehicle is the single-agent target, the green vehicles are the multi-agent targets, and the red vehicles are the non-scored surrounding agents. The same-colored lines following each agent represent the observed past trajectory, while the same-colored dotted lines preceding them indicate their future trajectory.

II. BACKGROUND

The focus on the *highD* [15], *round* [16], and *inD* [17] datasets is motivated by their high tracking accuracy, allowing for interpretable and reliable evaluations—making them particularly suitable for early-stage research and development. The data were collected at several fixed locations (intersections, roundabouts, *etc.*) across Germany. The datasets are made up of multiple recordings that contain both static and dynamic information, provided as `.csv` files. Of particular interest are the `tracks.csv` files, which contain the trajectory information of all objects in the scene. For later releases, like *inD* and *round*, recordings are also accompanied by a Lanelet 2 [27] file in `.osm` format, which can be used to extract semantic information about the scene.

A. Related Work

Although there are numerous examples of studies that utilize the Drone datasets for behavior prediction research [28]–[39], they are used differently, some of which is illustrated in Table I. These inconsistencies complicate the comparison of results across studies since making fair comparisons necessitates uniform conditions for all methods. Rather than advocating for one approach over another, we aim to propose a standard that reflects the most common practices in the field. As such, there is a connection between this work and the ones that organize challenges or workshops, *e.g.*, [20], [21], or [22], as they provide a clear specification of dataset partitioning and evaluation metrics.

TABLE I
TIME SPECIFICATIONS OF STUDIES USING THE DRONE DATASETS.

Study	Sampl. Time	Observ. Window	Pred. Horizon
[28]	1.0 s	5.0 s	5.0 s
[31]	0.4 s	1.2 s	3.2 s
[30], [32]	0.4 s	3.2 s	4.8 s
[35]	0.4 s	4.0 s	4.0 s
[29], [34], [36]–[38]	0.2 s	3.0 s	5.0 s
[39]	0.08 s	1.6 s	2.4 s

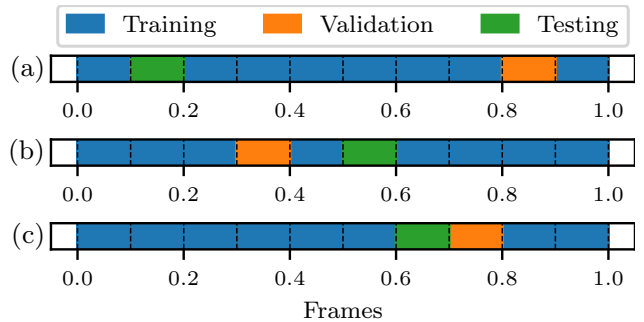


Fig. 2. Example of three different data splits, denoted by (a), (b), and (c), using the proposed partitioning method. The figure illustrates how the bins are divided into training, validation, and test sets based on the number of frames in each recording. The different colors are used to indicate which set each bin belongs to, where the dashed lines represent the boundaries between the bins.

III. PREPROCESSING

A. Prediction Objective

Resources for both single-agent and multi-agent trajectory prediction tasks are provided. In both cases, information on surrounding agents is supplied (should they exist) to encourage interaction-aware mechanisms. Motivated by the literature (see Table I), the observation window (length of the input sequence) is set to a maximum of 3 s, while the prediction horizon is set to 5 s. Each prediction scenario is centered around a target agent (TA), which also functions as the objective for the single-agent prediction task. The information on the single-agent target is always constructed to have maximum-length ground-truth data. To ensure consistency across scenarios, up to 8 nearest neighbors to the TA in the last observed frame are selected for the multi-agent prediction task—provided they have at least 3 s of future ground-truth data available. An example scenario is shown in Fig. 1.

B. Dataset Splits

Dataset partitioning is conducted at the recording level based on the number of frames in each file. For every recording, the total number of frames is partitioned into 10 equally sized bins, which are then randomly assigned to the training, validation, and test sets using a rough 80%-10%-10% split, as illustrated in Fig. 2. Since traffic behavior is highly dependent on the time of day, it is important to ensure that all partitions contain segments from various frames throughout the recordings to mitigate selection bias. The data extraction process then proceeds by collecting trajectories to construct scenarios from the recordings in the allocated time frames. We allow for overlapping scenarios between temporally adjacent bins belonging to the same partition to ensure that we gather as many samples as possible.

It is important to recognize that there is a notable imbalance across the maneuver classes within the *highD* dataset (the lane-change percentage is around 13%). To ensure that the scenarios are both dynamic and challenging, we adopt a stratified sampling approach, aiming to achieve a more balanced distribution of the TA maneuvers. Using the proposed preprocessing approach, the number of scenarios for each

partition and dataset is summarized in Table II, with the total number of trajectories shown in parentheses.

TABLE II
NUMBER OF SCENARIOS PER DATASET AND PARTITIONS.

Dataset	Training	Validation	Testing
<i>highD</i>	103,489 (1,532,748)	12,549 (184,787)	13,748 (202,499)
<i>roundD</i>	162,071 (1,793,089)	18,811 (209,376)	18,599 (204,420)
<i>inD</i>	103,587 (2,227,838)	12,232 (260,246)	11,781 (254,255)

C. Coordinate System

Although the Drone datasets are mostly consistent in terms of the data they provide, some differences need to be addressed, such as the coordinate system used. This is mainly an issue when working with the *highD* dataset. To ensure that the samples are consistent across the datasets, the data is first divided into two separate groups based on the direction of travel. Next, the data are transformed to a common coordinate system where the x -axis points in the direction of the road, the y -axis points to the left, and the origin is moved to the lower left corner of the road.

For the *roundD* and *inD* datasets, there are no such obvious issues, as all agents move in the same area. Regardless, we still place the origin in the approximate geographical center of the scene to ensure some consistency across recordings.

A possible issue, however, is that a global coordinate system could encourage prediction bias, where the predictor learns the patterns of a specific scene rather than a generalizable behavior model—an essential property for zero-shot learning [40], [41]. While we leave this design choice to the user, a possible approach could be to transform the scenario to a relative coordinate system, *e.g.*, the local coordinate system of the TA.

D. Downsampling

Most related works have used downsampling as a preprocessing step when working with the Drone datasets [28]–[39], albeit with different integer factors. Although there are several potential computational benefits—allowing for faster prototyping and experimentation—it is important to consider the qualitative effect downsampling has on both the data and the model. Figure 3 is used to illustrate how different sampling rates can affect the quality of predicted trajectories using nominal driving conditions for the *roundD* dataset. In the figure, we see that for lower sampling rates, the simulated trajectories become overly jagged and unrealistic, which makes it difficult to assess the physical feasibility of the predicted trajectories. To ensure that the data are still representative of the original tracking data, we propose to downsample it to a rate of 5 Hz, representing a sampling time of 0.2 s. When studying the frequency spectrum of the tracking data, it was found that several signals have components above the new Nyquist frequency (2.5 Hz). Before downsampling, an anti-aliasing filter is applied to remove these high-frequency components using a 7th order Chebyshev type I filter (based on qualitative evaluations).

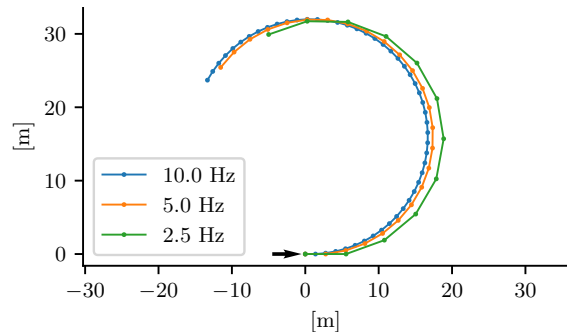


Fig. 3. Example simulation of a vehicle moving along a circular path with a radius of 16 m, a speed of 50 km/h (speed limit) for a duration of 5 s using different sampling rates in a forward Euler integration scheme. The values represent nominal conditions for the *roundD* dataset. The figure is used to illustrate how different sampling rates can affect motion prediction quality. Something that could be of interest when assessing the physical feasibility of the predicted trajectories.

TABLE III
AGENT FEATURES.

Feature	Description	Unit
x	Longitudinal coordinate	m
y	Lateral coordinate	m
v_x	Instantaneous longitudinal velocity	m/s
v_y	Instantaneous lateral velocity	m/s
ψ	Heading angle	rad
<i>Supplementary</i>		
a_x	Instantaneous longitudinal acceleration	m/s ²
a_y	Instantaneous lateral acceleration	m/s ²

E. Agent Features

1) *Tracking Features*: The Drone datasets contain a rich set of features for each agent, which are mostly consistent across the datasets. In Table III we list the type of features that are made available for each agent present in a sample scenario. The types of features available are the same in both the input and ground-truth target data. Importantly, the heading angle is not available in the *highD* dataset, and therefore estimated using the instantaneous velocities as

$$\psi = \arctan 2(v_y, v_x). \quad (1)$$

The longitudinal and lateral accelerations are included as supplementary features, *i.e.*, for development purposes. We argue against their inclusion in the final model since acceleration measurements are rarely available in POV data—they could of course serve a purpose in an extended ablation study.

2) *Agent Classes*: The different datasets contain agents of different types, *e.g.*, cars, bicycles, pedestrians, *etc.* We hypothesize that the model could benefit from the inclusion of this information, as different classes exhibit different behaviors. To allow for a more generalizable model, we propose a common set of agent classes across the datasets. In Table IV we list the agent classes and their corresponding values. The categories could be included as one-hot encoded features, or directly used as tokens in an embedding layer. The distribution of unique agents and their respective classes in the datasets is shown in Fig. 4.

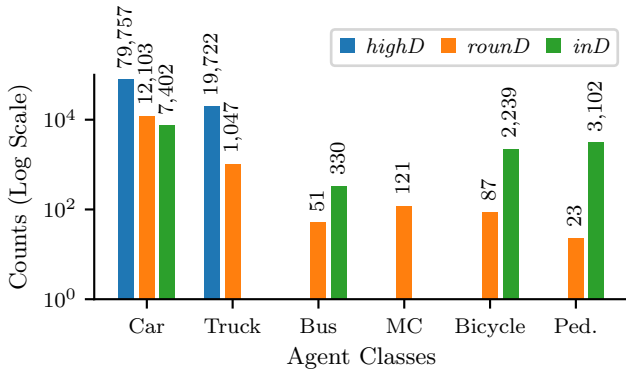


Fig. 4. Distribution of unique agent classes across the datasets.

TABLE IV
AGENT CLASSES.

Type	Car / Van	Truck	Bus	Motorcycle	Bicycle	Pedestrian
Value	0	1	2	3	4	5

F. Semantic Maps

With the emergence of datasets that include map-based information, the effort to incorporate such contextual knowledge into the learning process has gained notable attention [41]–[46]. However, how to best represent this information in a way that is both expressive and computationally efficient remains an open research question. One increasingly popular approach is to encode the semantics of the road network as a graph, with nodes representing geographical points of varying categories (*e.g.*, traffic lights, intersections, lane boundaries, lane markings, buildings, *etc.*) and edges representing the connections between these points. With the emerging interest in graph neural networks (GNNs) for trajectory prediction tasks [3], [47], this representation has shown to be effective in capturing the spatial dependencies between agents and the environment, while also ensuring consistent data modalities (as opposed to, *e.g.*, raw images or rasterized maps).

The recordings in the *rounD* and *inD* datasets are accompanied by Lanelet 2 [27] files that can be used to extract semantic information about the scenes. Our toolbox includes functionality for basic lane-graph construction, designed to serve as a foundation that users can modify according to their specific needs and preferences. Although the *highD* dataset does not include Lanelets, available information on the lane and road boundaries can be used to construct a simple lane graph. Example lane graphs are shown in Fig. 5.

G. Data Structure

As scenarios contain a variable number of agents, the toolbox uses PyG [25] when loading samples to handle this dimension inconsistency. An example batch of scenarios is illustrated in Listing 1. The batch object contains two heterogeneous graphs, one for the agents and one for the lane graph. The entries in the agent graph contain information on the agent features, masking tensors, and pointers to the batched data. It is important to note that although PyG components are included in our toolbox, this does not imply

```

1 HeteroDataBatch(
2   rec_id=[32],
3   agent={
4     num_nodes=350,
5     ta_index=[32],
6     atype=[350],
7     inp_pos=[350, 15, 2],
8     ...
9     trg_pos=[350, 25, 2],
10    ...
11    input_mask=[350, 15],
12    valid_mask=[350, 25],
13    sa_mask=[350, 25],
14    ma_mask=[350, 25],
15    batch=[350],
16    ptr=[33],
17  },
18  map_point={
19    num_nodes=14880,
20    mtype=[14880],
21    position=[14880, 2],
22    batch=[14880],
23    ptr=[33],
24  },
25  (map_point, to, map_point)={
26    edge_index=[2, 31744],
27    etype=[31744, 1],
28  }
29 )

```

Listing 1. Example batch of scenarios.

a requirement for users to incorporate GNNs into their model. PyG is only used for the convenience of handling the data.

IV. EVALUATION METRICS

In this section, we describe the metrics most commonly used in the literature to evaluate motion prediction models that are included in the toolbox. The metrics are here presented for a single agent but can easily be extended to multi-agent problems by averaging over all scored agents in the scenario. Here, $\mathbf{x}_k \in \mathbb{R}^2$ refers to the ground truth position at time step k , $\hat{\mathbf{x}}_k$ refers to the respective prediction, and N is the prediction horizon steps.

For multi-modal predictors, it is important to consider which of the prediction candidates should be used. A widely adopted approach is to use the prediction that is closest to the ground truth [3], [21], [22]. Although this disregards possibly predicted mode probability, it does allow for comparison with methods that do not directly parameterize independent modes, such as sampling-based generative models [8], [31], [46]. For completeness, we also include metrics that consider predicted distributions.

- *Average Displacement Error (ADE)*: The average L^2 -norm over the complete prediction horizon is

$$\text{ADE} = \frac{1}{N} \sum_{k=1}^N \|\hat{\mathbf{x}}_k - \mathbf{x}_k\|_2, \quad (2)$$

where the minimum ADE ($\min\text{ADE}_K$) is commonly used to indicate the minimum value over K predictions.

- *Final Displacement Error (FDE)*: The L^2 -norm of the final predicted position reflects the accuracy of the model

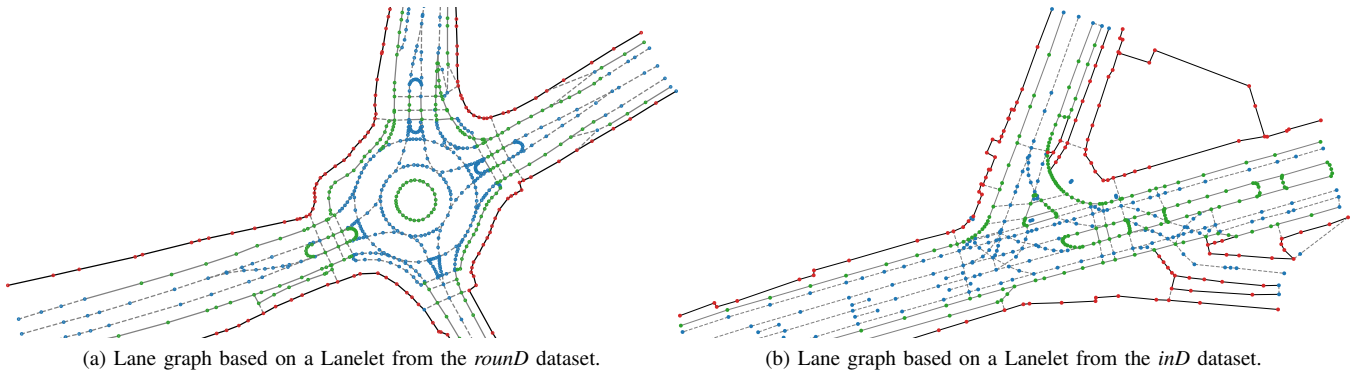


Fig. 5. Example lane graphs for the *roundD* and *inD* datasets. The lane graphs are constructed using the available Lanelet files, which contain semantic information about the scene. The lane graphs are constructed by extracting lane boundaries and markings, coloring them according to their type, and connecting them with edges. Although these examples are simple, combined with the available traffic data, they could be sufficient for many trajectory prediction tasks. Using the provided functionality, users can develop more complex lane graph constructions based on the desired detail level.

in forecasting distant future events

$$\text{FDE} = \|\hat{\mathbf{x}}_N - \mathbf{x}_N\|_2, \quad (3)$$

where the minimum FDE (minFDE_K) is commonly used to indicate the minimum value over K predictions.

- **Average Path Displacement Error (APDE):** The average minimum L^2 -norm between the predicted positions and the ground truth is used to estimate the path error. This can be used to determine predicted maneuver accuracy

$$\text{APDE} = \frac{1}{N} \sum_{k=1}^N \|\hat{\mathbf{x}}_k - \mathbf{x}_{k^*}\|_2 \quad (4)$$

$$k^* = \underset{i}{\text{argmin}} \|\hat{\mathbf{x}}_k - \mathbf{x}_i\|_2$$

- **Miss Rate (MR):** The ratio of cases where the predicted final position is not within 2 m of the ground truth is called the miss rate [3]. Although the 2 m threshold is derived from urban driving datasets, it has been shown to work well in highway scenarios as well [36], [46].
- **Collision Rate (CR):** The ratio of cases where for any timestep over the prediction horizon, the predicted position for another track was within 1 m is called the collision rate. Note that this is multi-agent specific and may not apply to all studies.
- **Brier Final Displacement Error (Brier-FDE):** The Brier-FDE is a metric that considers the final position of the predicted distribution [21], which is particularly useful for multi-modal predictors:

$$\text{FDE} = (1 - \pi^j)^2 \|\hat{\mathbf{x}}_N^j - \mathbf{x}_N\|_2, \quad (5)$$

where π^j is the predicted mode probability of the j -th mode.

- **Average Negative Log-Likelihood (ANLL):** This metric provides an estimate of how well the predicted distribution matches the observed data:

$$\text{ANLL} = \frac{1}{N} \sum_{k=1}^N -\log \mathcal{D}(\mathbf{x}_k | \hat{\mathbf{x}}_k), \quad (6)$$

where \mathcal{D} is the predicted distribution, commonly modeled as a mixture of Gaussian or Laplacian distributions [6], [29], [36], [45].

Minimum distance metrics are based on the mode with the lowest FDE in the toolbox to ensure that the evaluations are consistent with the chosen prediction.

V. FUTURE DIRECTIONS

The introduction of the toolbox for the development of trajectory-prediction models for the **Drone** datasets opens up several directions for future research. Here we outline some potential areas for further exploration.

- **Scenario-Specific Performance:** Investigate and compare model performance across the dataset suite to determine whether a model structure or hyperparameter configuration adopted to one scenario retains its accuracy in another.
- **Generalization & Zero-Shot Learning:** Explore model generalization and zero-shot learning across datasets to investigate how models can be applied or adapted across different scenarios.
- **Transfer Learning:** Explore the potential of applying models, initially trained on one or more **Drone** datasets with subsequent fine-tuning, to other datasets within the **Drone** suite or even to external datasets such as *INTERACTION*, *Argoverse 2*, or *WOMD*.

VI. CONCLUSIONS

This paper has presented a toolbox for the development of trajectory prediction models utilizing the **Drone** datasets. Based on the most common practices in the field, the toolbox is designed to standardize preprocessing and performance evaluation procedures, thereby simplifying comparative studies. By alleviating the technical burden of developing research pipelines, the toolbox augments the potential for exploration and discoveries in the field of trajectory prediction.

REFERENCES

- [1] S. Lefèvre, D. Vasquez, and C. Laugier, "A survey on motion prediction and risk assessment for intelligent vehicles," *ROBOMECH journal*, vol. 1, pp. 1–14, 2014.

- [2] S. Mozaffari, O. Y. Al-Jarrah, M. Dianati, P. Jennings, and A. Mouzakitis, "Deep learning-based vehicle behavior prediction for autonomous driving applications: A review," *IEEE Trans. Intell. Transport. Syst.*, vol. 23, no. 1, pp. 33–47, 2020.
- [3] Y. Huang, J. Du, Z. Yang, Z. Zhou, L. Zhang, and H. Chen, "A survey on trajectory-prediction methods for autonomous driving," *IEEE Trans. Intell. Veh.*, vol. 7, no. 3, pp. 652–674, 2022.
- [4] V. Alexiadis, J. Colyar, J. Halkias, R. Hranac, and G. McHale, "The next generation simulation program," *Inst. of Transp. Eng. Journal*, vol. 74, no. 8, p. 22, 2004.
- [5] D. J. Phillips, T. A. Wheeler, and M. J. Kochenderfer, "Generalizable intention prediction of human drivers at intersections," in *IEEE Intell. Veh. Symp.*, 2017, pp. 1665–1670.
- [6] N. Deo and M. M. Trivedi, "Convolutional social pooling for vehicle trajectory prediction," in *IEEE Conf. Comput. Vision Pattern Recog.*, 2018, pp. 1468–1476.
- [7] Y. Hu, W. Zhan, and M. Tomizuka, "Probabilistic prediction of vehicle semantic intention and motion," in *IEEE Intell. Veh. Symp.*, 2018, pp. 307–313.
- [8] T. Zhao, Y. Xu, M. Monfort, W. Choi, C. Baker, Y. Zhao, Y. Wang, and Y. N. Wu, "Multi-agent tensor fusion for contextual trajectory prediction," in *IEEE/CVF Conf. Comput. Vision Pattern Recog.*, 2019, pp. 12 126–12 134.
- [9] J. Mercat, T. Gilles, N. El Zoghby, G. Sandou, D. Beauvois, and G. P. Gil, "Multi-head attention for multi-modal joint vehicle motion forecasting," in *IEEE Int. Conf. Robot. Automat.*, 2020, pp. 9638–9644.
- [10] T. Westny, E. Frisk, and B. Olofsson, "Vehicle behavior prediction and generalization using imbalanced learning techniques," in *IEEE Intell. Transport. Syst. Conf.*, 2021, pp. 2003–2010.
- [11] M. Montanino and V. Punzo, "Making NGSIM data usable for studies on traffic flow theory: Multistep method for vehicle trajectory reconstruction," *Transp. Res. Rec.*, vol. 2390, no. 1, pp. 99–111, 2013.
- [12] B. Coifman and L. Li, "A critical evaluation of the Next Generation Simulation (NGSIM) vehicle trajectory dataset," *Transp. Research. Part B: Methodological*, vol. 105, pp. 362–377, 2017.
- [13] W. Zhan, L. Sun, D. Wang, H. Shi, A. Clausse, M. Naumann, J. Kümmerle, H. Königshof, C. Stiller, A. de La Fortelle, and M. Tomizuka, "INTERACTION Dataset: An INTERnational, Adversarial and Cooperative motion Dataset in Interactive Driving Scenarios with Semantic Maps," *arXiv:1910.03088 [cs, eess]*, 2019.
- [14] A. Robicquet, A. Sadeghian, A. Alahi, and S. Savarese, "Learning social etiquette: Human trajectory understanding in crowded scenes," in *Eur. Conf. Comput. Vision*, 2016, pp. 549–565.
- [15] R. Krajewski, J. Bock, L. Kloecker, and L. Eckstein, "The highD dataset: A drone dataset of naturalistic vehicle trajectories on German highways for validation of highly automated driving systems," in *IEEE Intell. Transport. Syst. Conf.*, 2018, pp. 2118–2125.
- [16] R. Krajewski, T. Moers, J. Bock, L. Vater, and L. Eckstein, "The roundD dataset: A drone dataset of road user trajectories at roundabouts in Germany," in *IEEE Intell. Transport. Syst. Conf.*, 2020, pp. 1–6.
- [17] J. Bock, R. Krajewski, T. Moers, S. Runde, L. Vater, and L. Eckstein, "The inD dataset: A drone dataset of naturalistic road user trajectories at German intersections," in *IEEE Intell. Veh. Symp.*, 2020, pp. 1929–1934.
- [18] T. Moers, L. Vater, R. Krajewski, J. Bock, A. Zlocki, and L. Eckstein, "The exiD dataset: A real-world trajectory dataset of highly interactive highway scenarios in Germany," in *IEEE Intell. Veh. Symp.*, 2022, pp. 958–964.
- [19] V. Ramanishka, Y.-T. Chen, T. Misu, and K. Saenko, "Toward driving scene understanding: A dataset for learning driver behavior and causal reasoning," in *IEEE Conf. Comput. Vision Pattern Recog.*, 2018, pp. 7699–7707.
- [20] H. Caesar, V. Bankiti, A. H. Lang, S. Vora, V. E. Liong, Q. Xu, A. Krishnan, Y. Pan, G. Baldan, and O. Beijbom, "NuScenes: A multimodal dataset for autonomous driving," in *IEEE/CVF Conf. Comput. Vision Pattern Recog.*, 2020, pp. 11 621–11 631.
- [21] B. Wilson, W. Qi, T. Agarwal, J. Lambert, J. Singh, S. Khandelwal, B. Pan, R. Kumar, A. Hartnett, J. K. Pontes, D. Ramanan, P. Carr, and J. Hays, "Argoverse 2: Next generation datasets for self-driving perception and forecasting," in *Neural Inform. Proc. Syst. Track on Datasets and Benchmarks*, 2021.
- [22] S. Ettinger, S. Cheng, B. Caine, C. Liu, H. Zhao, S. Pradhan, Y. Chai, B. Sapp, C. R. Qi, Y. Zhou, *et al.*, "Large scale interactive motion forecasting for autonomous driving: The Waymo open motion dataset," in *IEEE/CVF Int. Conf. Comput. Vision*, 2021, pp. 9710–9719.
- [23] "CVPR 2023 Workshop on Autonomous Driving," <https://cvpr2023.wad.vision/>, [Online]; accessed April 6th 2024.
- [24] A. Paszke, S. Gross, F. Massa, A. Lerer, J. Bradbury, G. Chanan, T. Killeen, Z. Lin, N. Gimelshein, L. Antiga, *et al.*, "PyTorch: An imperative style, high-performance deep learning library," in *Int. Conf. Adv. in Neural Inf. Process. Syst.*, 2019.
- [25] M. Fey and J. E. Lenssen, "Fast graph representation learning with PyTorch Geometric," in *ICLR Workshop on Representation Learn. on Graphs and Manifolds*, 2019.
- [26] W. Falcon and The PyTorch Lightning team, "PyTorch Lightning," Mar. 2019. [Online]. Available: <https://github.com/Lightning-AI/lightning>
- [27] F. Poggendorf, J.-H. Pauls, J. Janosovits, S. Orf, M. Naumann, F. Kuhnt, and M. Mayr, "Lanelet2: A high-definition map framework for the future of automated driving," in *IEEE Intell. Transport. Syst. Conf.*, 2018, pp. 1672–1679.
- [28] F. Diehl, T. Brunner, M. T. Le, and A. Knoll, "Graph neural networks for modelling traffic participant interaction," in *IEEE Intell. Veh. Symp.*, 2019, pp. 695–701.
- [29] K. Messaoud, I. Yahiaoui, A. Verroust-Blondet, and F. Nashashibi, "Attention based vehicle trajectory prediction," *IEEE Trans. Intell. Veh.*, vol. 6, no. 1, pp. 175–185, 2021.
- [30] S. Carrasco, D. F. Llorca, and M. Sotelo, "SCOUT: Socially-consistent and understandable graph attention network for trajectory prediction of vehicles and VRUs," in *IEEE Intell. Veh. Symp.*, 2021, pp. 1501–1508.
- [31] H. Ma, Y. Sun, J. Li, M. Tomizuka, and C. Choi, "Continual multi-agent interaction behavior prediction with conditional generative memory," *IEEE Robot. Automat. Lett.*, vol. 6, no. 4, pp. 8410–8417, 2021.
- [32] H. Cheng, W. Liao, X. Tang, M. Y. Yang, M. Sester, and B. Rosenhahn, "Exploring dynamic context for multi-path trajectory prediction," in *IEEE Int. Conf. Robot. Automat.*, 2021, pp. 12 795–12 801.
- [33] A. Quintanar, D. Fernández-Llorca, I. Parra, R. Izquierdo, and M. Sotelo, "Predicting vehicles trajectories in urban scenarios with transformer networks and augmented information," in *IEEE Intell. Veh. Symp.*, 2021, pp. 1051–1056.
- [34] X. Chen, H. Zhang, F. Zhao, Y. Hu, C. Tan, and J. Yang, "Intention-aware vehicle trajectory prediction based on spatial-temporal dynamic attention network for internet of vehicles," *IEEE Trans. Intell. Transport. Syst.*, vol. 23, no. 10, pp. 19 471–19 483, 2022.
- [35] S. Wen, H. Wang, and D. Metaxas, "Social ODE: Multi-agent trajectory forecasting with neural ordinary differential equations," in *Eur. Conf. Comput. Vision*, 2022, pp. 217–233.
- [36] T. Westny, J. Oskarsson, B. Olofsson, and E. Frisk, "MTP-GO: Graph-based probabilistic multi-agent trajectory prediction with neural ODEs," *IEEE Trans. Intell. Veh.*, vol. 8, no. 9, pp. 4223–4236, 2023.
- [37] ———, "Evaluation of differentially constrained motion models for graph-based trajectory prediction," in *IEEE Intell. Veh. Symp.*, 2023.
- [38] S. Mozaffari, M. A. Sormoli, K. Koufos, and M. Dianati, "Multimodal manoeuvre and trajectory prediction for automated driving on highways using transformer networks," *IEEE Robot. Automat. Lett.*, vol. 8, no. 10, pp. 6123–6130, 2023.
- [39] Z. Wang, J. Zhang, J. Chen, and H. Zhang, "Spatio-temporal context graph transformer design for map-free multi-agent trajectory prediction," *IEEE Trans. Intell. Veh.*, vol. 9, no. 1, pp. 1369–1381, 2024.
- [40] N. Jaipuria, G. Habibi, and J. P. How, "Learning in the curbside coordinate frame for a transferable pedestrian trajectory prediction model," in *IEEE Intell. Transport. Syst. Conf.*, 2018, pp. 3125–3131.
- [41] Y. Hu, W. Zhan, and M. Tomizuka, "Scenario-transferable semantic graph reasoning for interaction-aware probabilistic prediction," *IEEE Trans. Intell. Transport. Syst.*, vol. 23, no. 12, pp. 23 212–23 230, 2022.
- [42] M. Liang, B. Yang, R. Hu, Y. Chen, R. Liao, S. Feng, and R. Urtasun, "Learning lane graph representations for motion forecasting," in *Eur. Conf. Comput. Vision*, 2020, pp. 541–556.
- [43] T. Salzmann, B. Ivanovic, P. Chakravarty, and M. Pavone, "Trajectory++: Dynamically-feasible trajectory forecasting with heterogeneous data," in *Eur. Conf. Comput. Vision*, 2020, pp. 683–700.
- [44] N. Deo, E. Wolff, and O. Beijbom, "Multimodal trajectory prediction conditioned on lane-graph traversals," in *Conf. on Robot Learn.* PMLR, 2022, pp. 203–212.
- [45] Z. Zhou, J. Wang, Y.-H. Li, and Y.-K. Huang, "Query-centric trajectory prediction," in *IEEE/CVF Conf. Comput. Vision Pattern Recog.*, 2023, pp. 17 863–17 873.
- [46] T. Westny, B. Olofsson, and E. Frisk, "Diffusion-based environment-aware trajectory prediction," *arXiv preprint arXiv:2403.11643*, 2024.
- [47] S. Rahmani, A. Baghbani, N. Bouguila, and Z. Patterson, "Graph neural networks for intelligent transportation systems: A survey," *IEEE Trans. Intell. Transport. Syst.*, vol. 24, no. 8, pp. 8846–8885, 2023.